

## Study of photon strength functions of $^{241}\text{Pu}$ and $^{245}\text{Cm}$ from neutron capture measurements

*E. Mendoza<sup>1,\*</sup>, V. Alcayne<sup>1</sup>, D. Cano-Ott<sup>1</sup>, A. Kimura<sup>2</sup>, A. V. Skarbeli<sup>1</sup>, O. Aberle<sup>3</sup>, S. Amaducci<sup>4,5</sup>, J. Andrzejewski<sup>6</sup>, L. Audouin<sup>7</sup>, V. Babiano-Suarez<sup>8</sup>, M. Bacak<sup>3,9,10</sup>, M. Barbagallo<sup>3,11</sup>, V. Bécaries<sup>1</sup>, F. Bečvář<sup>12</sup>, G. Bellia<sup>4,5</sup>, E. Berthoumieux<sup>10</sup>, J. Billowes<sup>13</sup>, D. Bosnar<sup>14</sup>, A. S. Brown<sup>15</sup>, M. Busso<sup>16,17</sup>, M. Caamaño<sup>18</sup>, L. Caballero<sup>8</sup>, M. Calviani<sup>3</sup>, F. Calviño<sup>19</sup>, A. Casanovas<sup>19</sup>, F. Cerutti<sup>3</sup>, Y. H. Chen<sup>7</sup>, E. Chiaveri<sup>13,20,3</sup>, N. Colonna<sup>11</sup>, G. P. Cortés<sup>19</sup>, M. A. Cortés-Giraldo<sup>20</sup>, L. Cosentino<sup>4</sup>, S. Cristallo<sup>16,21</sup>, L. A. Damone<sup>11,22</sup>, M. Diakaki<sup>23</sup>, M. Dietz<sup>24</sup>, C. Domingo-Pardo<sup>8</sup>, R. Dressler<sup>25</sup>, E. Dupont<sup>10</sup>, I. Durán<sup>18</sup>, Z. Eleme<sup>26</sup>, B. Fernández-Domínguez<sup>18</sup>, A. Ferrari<sup>3</sup>, I. Ferro-Gonçalves<sup>27</sup>, P. Finocchiaro<sup>4</sup>, V. Furman<sup>28</sup>, R. Garg<sup>24</sup>, A. Gawlik<sup>6</sup>, S. Gilardoni<sup>3</sup>, T. Glodariu<sup>29</sup>, K. Göbel<sup>30</sup>, E. González-Romero<sup>1</sup>, C. Guerrero<sup>20</sup>, F. Gunsing<sup>10</sup>, S. Heinitz<sup>25</sup>, J. Heyse<sup>31</sup>, D. G. Jenkins<sup>15</sup>, E. Jericha<sup>9</sup>, Y. Kadi<sup>3</sup>, F. Käppeler<sup>32</sup>, N. Kivel<sup>25</sup>, M. Kokkoris<sup>23</sup>, Y. Kopatch<sup>28</sup>, M. Krtička<sup>12</sup>, D. Kurtulgil<sup>30</sup>, I. Ladarescu<sup>8</sup>, C. Lederer-Woods<sup>24</sup>, J. Lerendegui-Marco<sup>20</sup>, S. Lo Meo<sup>33,34</sup>, S.-J. Lonsdale<sup>24</sup>, D. Macina<sup>3</sup>, A. Manna<sup>34,35</sup>, T. Martínez<sup>1</sup>, A. Masi<sup>3</sup>, C. Massimi<sup>34,35</sup>, P. F. Mastinu<sup>36</sup>, M. Mastromarco<sup>3,13</sup>, F. Matteucci<sup>37,38</sup>, E. Mauger<sup>25</sup>, A. Mazzone<sup>11,39</sup>, A. Mengoni<sup>33,34</sup>, V. Michalopoulou<sup>23</sup>, P. M. Milazzo<sup>37</sup>, F. Mingrone<sup>3</sup>, A. Musumarra<sup>4,5</sup>, A. Negret<sup>29</sup>, R. Nolte<sup>40</sup>, F. Ogállar<sup>41</sup>, A. Oprea<sup>29</sup>, N. Patronis<sup>26</sup>, A. Pavlik<sup>42</sup>, J. Perkowski<sup>6</sup>, L. Piersanti<sup>16,21</sup>, I. Porras<sup>41</sup>, J. Praena<sup>41</sup>, J. M. Quesada<sup>20</sup>, D. Radeck<sup>40</sup>, D. Ramos Doval<sup>7</sup>, R. Reifarth<sup>30</sup>, D. Rochman<sup>25</sup>, C. Rubbia<sup>3</sup>, M. Sabaté-Gilarte<sup>20,3</sup>, A. Saxena<sup>43</sup>, P. Schillebeeckx<sup>31</sup>, D. Schumann<sup>25</sup>, A. G. Smith<sup>13</sup>, N. Sosnin<sup>13</sup>, A. Stamatopoulos<sup>23</sup>, G. Tagliente<sup>11</sup>, J. L. Tain<sup>8</sup>, Z. Talip<sup>25</sup>, A. E. Tarifeño-Saldivia<sup>19</sup>, L. Tassan-Got<sup>3,23,7</sup>, P. Torres-Sánchez<sup>41</sup>, A. Tsinganis<sup>3</sup>, J. Ulrich<sup>25</sup>, S. Urlass<sup>3,44</sup>, S. Valenta<sup>12</sup>, G. Vannini<sup>34,35</sup>, V. Variale<sup>11</sup>, P. Vaz<sup>27</sup>, A. Ventura<sup>34</sup>, V. Vlachoudis<sup>3</sup>, R. Vlastou<sup>23</sup>, A. Wallner<sup>45</sup>, P. J. Woods<sup>24</sup>, T. J. Wright<sup>13</sup>, and P. Žugec<sup>14</sup>*

<sup>1</sup>Centro de Investigaciones Energéticas Medioambientales y Tecnológicas (CIEMAT), Spain

<sup>2</sup>Japan Atomic Energy Agency (JAEA), Tokai-mura, Japan

<sup>3</sup>European Organization for Nuclear Research (CERN), Switzerland

<sup>4</sup>INFN Laboratori Nazionali del Sud, Catania, Italy

<sup>5</sup>Dipartimento di Fisica e Astronomia, Università di Catania, Italy

<sup>6</sup>University of Lodz, Poland

<sup>7</sup>IPN, CNRS-IN2P3, Univ. Paris-Sud, Université Paris-Saclay, F-91406 Orsay Cedex, France

<sup>8</sup>Instituto de Física Corpuscular, CSIC - Universidad de Valencia, Spain

<sup>9</sup>Technische Universität Wien, Austria

<sup>10</sup>CEA Saclay, Irfu, Université Paris-Saclay, Gif-sur-Yvette, France

<sup>11</sup>Istituto Nazionale di Fisica Nucleare, Bari, Italy

<sup>12</sup>Charles University, Prague, Czech Republic

<sup>13</sup>University of Manchester, United Kingdom

<sup>14</sup>Department of Physics, Faculty of Science, University of Zagreb, Croatia

<sup>15</sup>University of York, United Kingdom

<sup>16</sup>Istituto Nazionale di Fisica Nucleare, Perugia, Italy

<sup>17</sup>Dipartimento di Fisica e Geologia, Università di Perugia, Italy

<sup>18</sup>University of Santiago de Compostela, Spain

<sup>19</sup>Universitat Politècnica de Catalunya, Spain

<sup>20</sup>Universidad de Sevilla, Spain

<sup>21</sup>Istituto Nazionale di Astrofisica - Osservatorio Astronomico d'Abruzzo, Italy

<sup>22</sup>Dipartimento di Fisica, Università degli Studi di Bari, Italy

<sup>23</sup>National Technical University of Athens, Greece

<sup>24</sup>School of Physics and Astronomy, University of Edinburgh, United Kingdom

<sup>25</sup>Paul Scherrer Institut (PSI), Villigen, Switzerland

<sup>26</sup>University of Ioannina, Greece

<sup>27</sup>Instituto Superior Técnico, Lisbon, Portugal

<sup>28</sup>Joint Institute for Nuclear Research (JINR), Dubna, Russia

<sup>29</sup>Horia Hulubei National Institute of Physics and Nuclear Engineering (IFIN-HH), Bucharest

<sup>30</sup>Goethe University Frankfurt, Germany

<sup>31</sup>European Commission, Joint Research Centre, Geel, Retieseweg 111, B-2440 Geel, Belgium

<sup>32</sup>Karlsruhe Institute of Technology, Campus North, IKP, 76021 Karlsruhe, Germany

<sup>33</sup>Agenzia nazionale per le nuove tecnologie, l'energia e lo sviluppo economico sostenibile (ENEA), Bologna, Italy

<sup>34</sup>Istituto Nazionale di Fisica Nucleare, Sezione di Bologna, Italy

<sup>35</sup>Dipartimento di Fisica e Astronomia, Università di Bologna, Italy

<sup>36</sup>Istituto Nazionale di Fisica Nucleare, Sezione di Legnaro, Italy

<sup>37</sup>Istituto Nazionale di Fisica Nucleare, Trieste, Italy

<sup>38</sup>Dipartimento di Fisica, Università di Trieste, Italy

<sup>39</sup>Consiglio Nazionale delle Ricerche, Bari, Italy

<sup>40</sup>Physikalisch-Technische Bundesanstalt (PTB), Bundesallee 100, 38116 Braunschweig, Germany

<sup>41</sup>University of Granada, Spain

<sup>42</sup>University of Vienna, Faculty of Physics, Vienna, Austria

<sup>43</sup>Bhabha Atomic Research Centre (BARC), India

<sup>44</sup>Helmholtz-Zentrum Dresden-Rossendorf, Germany

<sup>45</sup>Australian National University, Canberra, Australia

### Abstract.

We have measured the  $\gamma$ -rays following neutron capture on  $^{240}\text{Pu}$  and  $^{244}\text{Cm}$  at the n\_TOF facility at CERN with the Total Absorption Calorimeter (TAC) and with  $\text{C}_6\text{D}_6$  organic scintillators. The TAC is made of 40  $\text{BaF}_2$  crystals operating in coincidence and covering almost the entire solid angle. This allows to obtain information concerning the energy spectra and the multiplicity of the measured capture  $\gamma$ -ray cascades. Additional information is also obtained from the  $\text{C}_6\text{D}_6$  detectors. We have analyzed the measured data in order to draw conclusions about the Photon Strength Functions (PSFs) of  $^{241}\text{Pu}$  and  $^{245}\text{Cm}$  below their neutron separation energies. The analysis has been performed by fitting the PSFs to the experimental results, using the differential evolution method, in order to find neutron capture cascades capable of reproducing at the same time a great variety of deposited energy spectra.

## 1 Introduction

We have measured the  $^{240}\text{Pu}$  and  $^{244}\text{Cm}$  neutron capture cross sections at the n\_TOF facility at CERN [1]. Both isotopes were present in the same sample, containing  $\sim 0.4$  mg  $^{240}\text{Pu}$  and  $\sim 0.8$  mg  $^{244}\text{Cm}$ . The measurement was performed in the two n\_TOF experimental areas. In the Experimental Area 1 (EAR-1) [1] we used the  $\text{BaF}_2$  Total Absorption Calorimeter (TAC) [2] for detecting the  $\gamma$ -rays emitted after neutron capture, and in the Experimental Area 2 (EAR-2) [3] we used three  $\text{C}_6\text{D}_6$  liquid scintillators. Details of the experimental setup can be found in [4].

The main goal of the measurement was to obtain the neutron capture cross section of  $^{244}\text{Cm}$ . However, as an additional result, the data are also useful for studying the  $\gamma$ -ray cascades following the  $^{240}\text{Pu}(n,\gamma)$  and  $^{244}\text{Cm}(n,\gamma)$  reactions. This has been already done for other actinides in previous studies from measurements performed at n\_TOF with the TAC [5–10] and with  $\text{C}_6\text{D}_6$  detectors [11], and from measurements performed at LANSCE [12] with the  $\text{BaF}_2$  Detector for Advanced Neutron Capture Experiments (DANCE) [13–15].

All these studies use a similar methodology. The electromagnetic cascades following neutron capture are obtained from the DICEBOX [16] or the DEGEN [17] codes. Then, the transport of these cascades through the detectors are simulated with detailed Geant4 [18] models to account for the detector response [19, 20]. Finally, the results of the simulations are compared with the experimental data. Both DICEBOX and DEGEN codes reconstruct the full level scheme and branching ratios of the compound nucleus for generating the cascades. They use the experimental data available in ENSDF [21] at low excitation energies, and statistical models to generate the rest of the level scheme and branching ratios. These models use level density formulas and Photon Strength Functions (PSFs),

which are varied until the simulations reproduce the experimental results. Electron conversion processes are included as well.

The adjustment of the PSFs to reproduce the experimental results has been done in all the works mentioned above *by hand*. That is, starting with values obtained in a previous work or with theoretical values normally taken from the RIPL-3 library [22], and modifying them little by little until satisfactory results are achieved. For the study of the cascades following the  $^{240}\text{Pu}(n,\gamma)$  and  $^{244}\text{Cm}(n,\gamma)$  reactions, i.e. the study of the  $^{241}\text{Pu}$  and  $^{245}\text{Cm}$  PSFs, we have investigated a different methodology. Instead of adjusting the PSFs *by hand* what we have done is to *fit* them, with a minimization algorithm, to reproduce the experimental data.

## 2 Description of the methodology

We have addressed the problem of finding PSFs that reproduce the experimental data as a minimization problem. The idea is to parameterize the PSFs, so  $PSFs = PSFs(\lambda_1, \lambda_2, \dots, \lambda_n)$ , where  $\lambda_1, \lambda_2, \dots, \lambda_n$  are the  $n$  parameters which define the PSFs, and build from these parameters a scalar function of  $n$  variables indicating how well the experimental data are reproduced. The lower the values of this function, hereafter referred as  $FOM = FOM(\lambda_1, \lambda_2, \dots, \lambda_n)$ , referring to Figure Of Merit, the better the experimental results are reproduced. The problem is therefore reduced to fit the  $\lambda$ -parameters to minimize the  $FOM$  function.

In order to obtain the value of the  $FOM$  function for a given set of parameters  $(\lambda_1, \lambda_2, \dots, \lambda_n)$  it is necessary to: (i) generate the cascades according to the corresponding PSFs; (ii) transport them through the detector geometry; (iii) reconstruct the simulated data in the same way as in the real experiment; and (iv) compare them with the experimental results.

\*e-mail: emilio.mendoza@ciemat.es

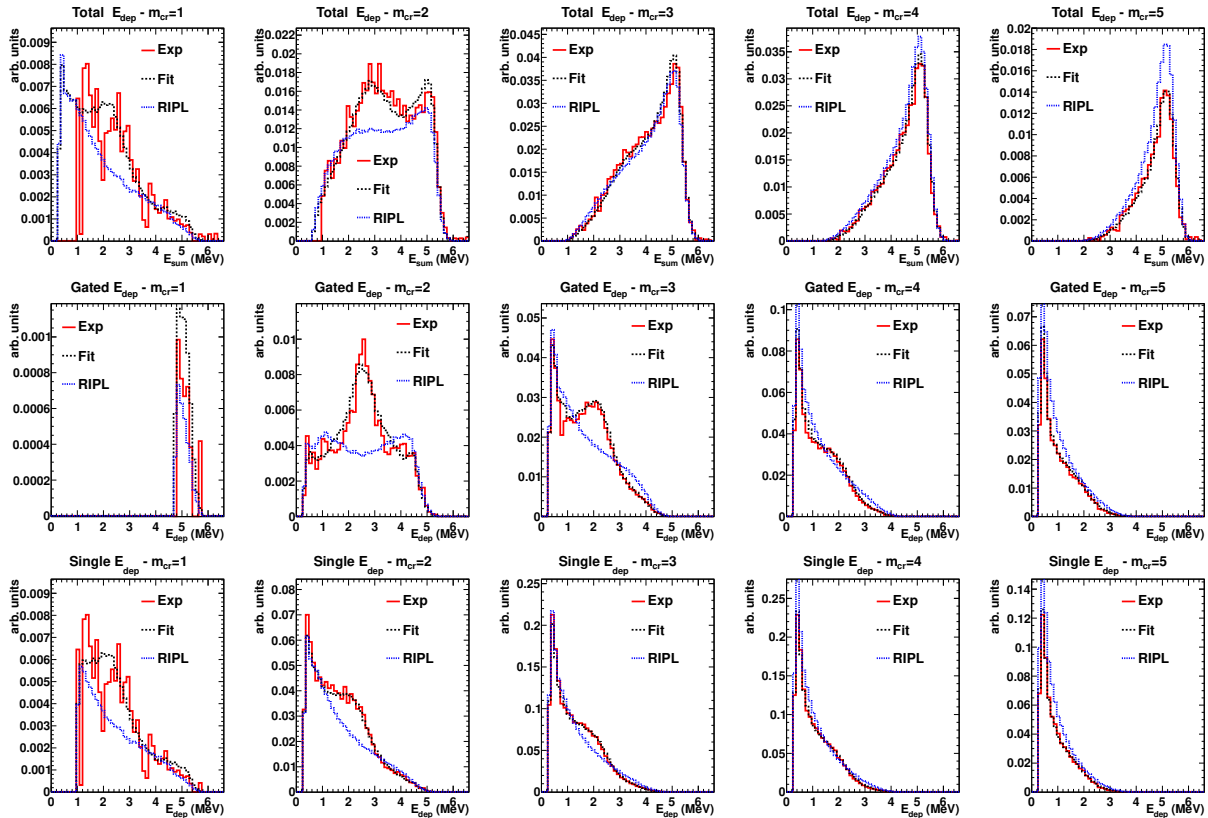


**Figure 1.** Comparison between experimental and simulated deposited energy spectra in the TAC for  $^{244}\text{Cm}(n,\gamma)$  cascades. We show spectra of three different types: the experimental ones (Exp), the simulated ones with the RIPL-3 PSFs (RIPL), and the simulated ones after fitting the PSFs (Fit). The panels at the top correspond to total deposited energy spectra, i.e. the sum of the energies deposited in the detectors in coincidence ( $E_{sum}$ ). The panels in the middle and at the bottom correspond to the deposited energy spectra in the individual  $\text{BaF}_2$  crystals (not in coincidence). In the panels in the middle, only detector signals contributing to events with total energy between 4.75 and 5.75 MeV have been considered. In all the cases there is also a condition in the crystal multiplicity ( $m_{cr}$ ), ranging from  $m_{cr} = 1$  (left, only one detector *in coincidence*) to  $m_{cr} = 5$  (right, five detectors in coincidence).

Instead of DICEBOX or DEGEN, we have used NuDEX [23] for the generation of the capture cascades. This code, which has been developed recently, works in a very similar way as the aforementioned codes do. We have used the experimental data from the TAC to perform the fit since we assumed that its response function is more sensitive to the *shape* of the cascade than the ones from the  $\text{C}_6\text{D}_6\text{s}$ . We have used the same Geant4 application as in previous works [19]. For the comparison with the experimental results, we have evaluated at the same time the reduced chi-squared of several different deposited energy spectra. The *FOM* has been defined as a linear combination of the resulting values.

For the fitting process, we have used the differential evolution algorithm [24–26], which presents numerous advantages for the problem we want to solve: it does not use derivatives, it is robust, easy to implement, and it can be easily used in parallel computing.

### 3 Results

Due to the small sample mass only the strongest resonances of  $^{240}\text{Pu}$  (at 1.06 eV) and  $^{244}\text{Cm}$  (at 7.67 eV) gave

rise to deposited energy spectra with sufficient statistics for the study of the cascades.

For the moment, we have used basically two types of parametrizations. One is similar to those used in previous works, which consists of parameterizing the PSFs according to a sum of resonances, usually of the Lorentzian-type. The parameters are in this case the ones defining the resonances (energy, width and intensity). The other is to define them as point-to-point functions, so that the parameters are the values of the PSFs at certain fixed points.

As an example, we present the results of a fit in Figure 1. There we show different deposited energy spectra in the TAC for  $^{244}\text{Cm}(n,\gamma)$  cascades. In the TAC the individual signals are grouped into *events* using a coincidence window. Each event is characterized by its time-of-flight, total deposited energy ( $E_{sum}$ ) and crystal multiplicity ( $m_{cr}$ ), which is the number of detectors contributing to an event. The five panels at the top (Total  $E_{dep}$ ) show the total deposited energy spectra, where the sum peak corresponds to the neutron separation energy in  $^{245}\text{Cm}$ ; the five panels in the middle (Gated  $E_{dep}$ ) show the individual crystal energy spectra obtained by gating on the  $4.75 < E_{sum} < 5.75$  MeV region; and the five panels at the

bottom (Single  $E_{dep}$ ) show the individual crystal energy spectra obtained without any gating. In all these cases the spectra correspond to  $m_{cr}$  ranging from one (left) to five (right). The simulations have been normalized to the total energy ( $E_{sum}$ ) experimental spectra (no cuts in  $m_{cr}$ ) between 2 and 6 MeV.

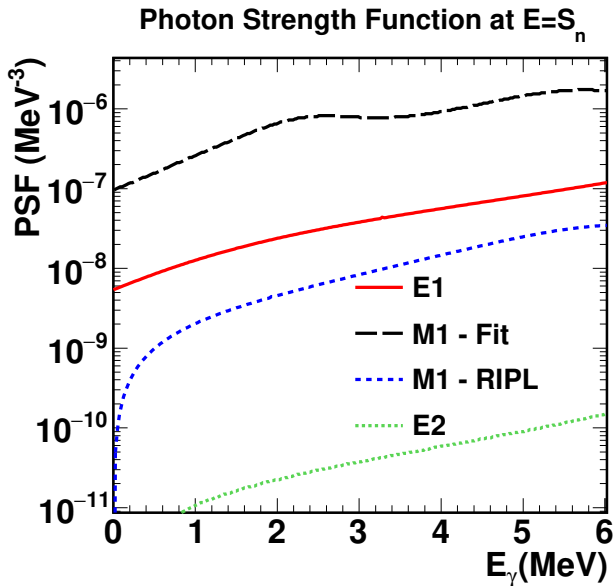


**Figure 2.** PSFs for  $^{245}\text{Cm}$  used in the simulations shown in Figure 1.

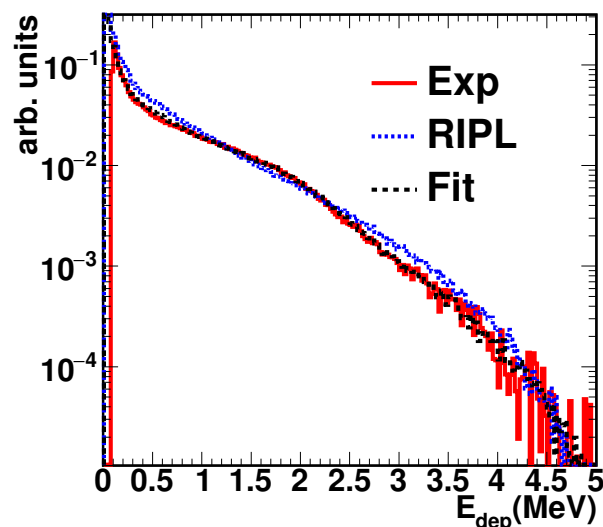


**Figure 3.** Deposited energy spectra in the  $\text{C}_6\text{D}_6$  detectors from  $^{244}\text{Cm}(n,\gamma)$  cascades. The experimental spectrum (Exp) is compared with the simulated spectrum obtained with the RIPL-3 PSFs (RIPL) and with the fitted PSF presented in Figures 1 and 2 (Fit).

In this case we have varied the M1 strength function only, by adding two resonances to the RIPL-3 M1-PSF. In

this way, six parameters have been fitted: three for each resonance (energy, width and intensity). The RIPL E1-PSF was modelled with two resonances using the modified Lorentzian model (MLO1 in [22]); and the RIPL-3 M1 and E2 PSFs with one resonance each, using the Standard Lorentzian model (SLO in [22]). The recommendations described in [22] were used to calculate the parameters of all these resonances. The *FOM* has been defined as the weighted sum of the 15 reduced chi-squared values obtained from the 15 spectra in Figure 1. The reduced chi-squared values of the total deposited energy spectra (the five at the top) have been weighted by a factor of 0.1, and the rest by a factor of 0.05. Figure 2 shows the results of the fit, in which the fitted M1-PSF is two order of magnitude larger than the one from RIPL-3. This PSF probably does not correspond to reality, since it is expected that E1 transitions dominate over M1 transitions, and also because it will lead to a too large  $\Gamma_\gamma$ , but it allows reproducing a large number of deposited experimental spectra. More work will be done in the future to study whether there are other solutions capable of reproducing the experimental spectra.

The same electromagnetic cascades fitted with the TAC spectra have been simulated in the  $\text{C}_6\text{D}_6$  experimental setup. The comparison with the experimental data is presented in Figure 3. There we see how the cascades fitted to reproduce the TAC response to  $^{244}\text{Cm}(n,\gamma)$  cascades perfectly reproduce the deposited energy spectra in the  $\text{C}_6\text{D}_6$  detectors as well.

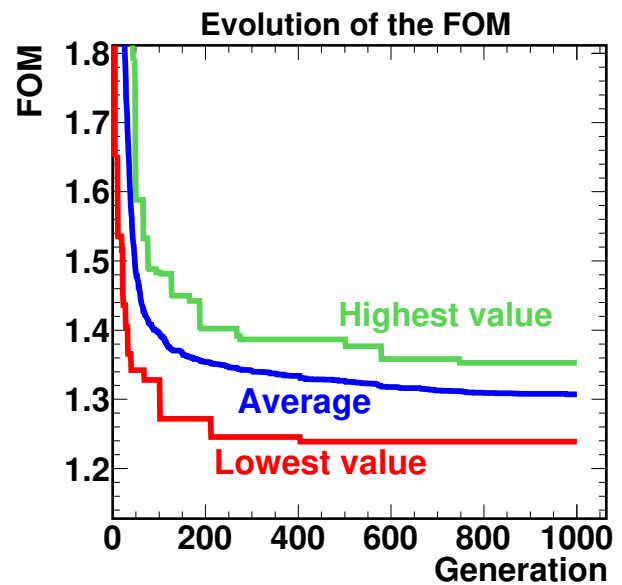


**Figure 4.** Evolution of the *FOM* as a function of the generation. The figure shows the highest and lowest *FOM* values for each generation together with the average value of all agents.

Concerning the convergence of the fitting process, differential evolution is a fitting method in which there are a number of candidate solutions, called *agents*, that are improving iteratively (more details in [24–26]). We show an example of evolution of the *FOM* as a function of the iter-

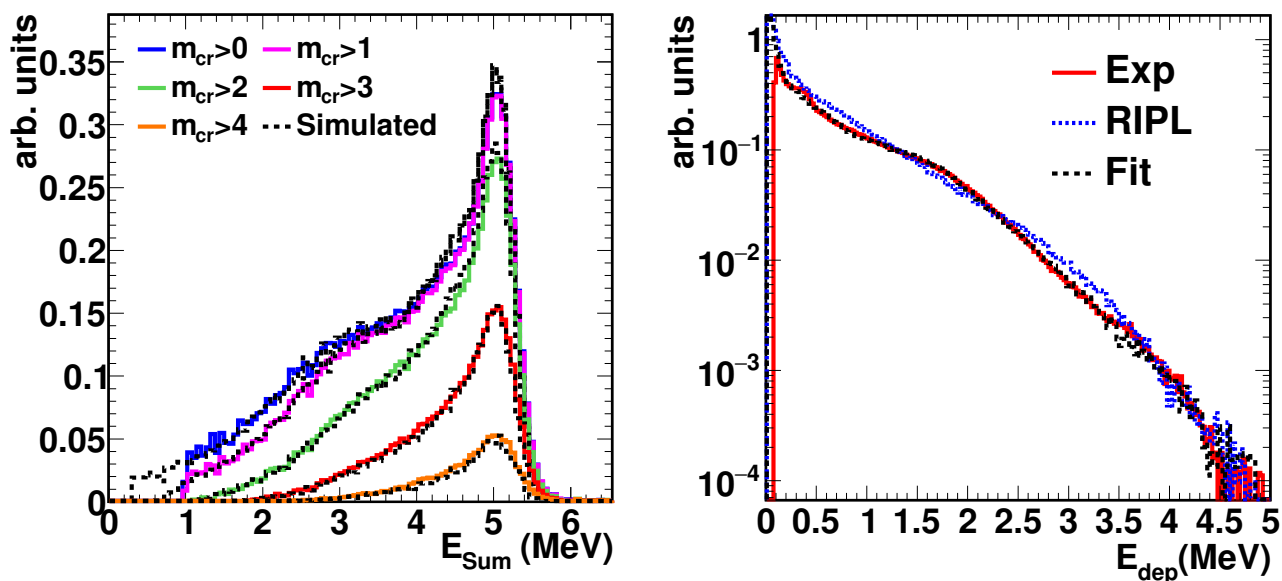


**Figure 5.** Comparison between experimental and simulated deposited energy spectra in the TAC (left) and in the  $C_6D_6$ s (right) for  $^{240}\text{Pu}(n,\gamma)$  cascades.

ation number (*generation*) in Figure 4. This fit is the one we have taken as an example in this section, and therefore has 6 free parameters. We have always used a number of agents which is ten times the number of free parameters, so in this case we have used 60 agents. The convergence is quite fast up to generation 100-200, and then the candidate solutions improve much more slowly. With more free parameters, the method takes longer to converge.

We have also found with this fitting method  $^{240}\text{Pu}(n,\gamma)$  cascades that reproduce the experimental results quite well, although they are not yet at the level of those of  $^{244}\text{Cm}(n,\gamma)$ . We show the result of a fit as an example in Figure 5. As in the previous case, the PSFs have been fitted to reproduce the TAC data and the resulting cascades have been simulated in the  $C_6D_6$  experimental setup. Again, we have modified the M1-PSF and the fit has converged to a solution much larger than the one proposed by RIPL-3, as in the previous case.

## 4 Conclusions

We have used the differential evolution fitting method to find neutron capture cascades capable of reproducing at the same time a great variety of deposited energy spectra. This methodology has been successfully applied to the specific cases of the  $^{240}\text{Pu}(n,\gamma)$  and  $^{244}\text{Cm}(n,\gamma)$  reactions. The knowledge of these cascades are fundamental for the analysis of capture cross section measurements, since it allows to calculate the detection efficiency by means of Monte Carlo simulations [6–9], or to make important corrections when applying the Pulse Height Weighting Technique [11]. Beyond these needs for analyzing the data, the study of PSFs is a field of research in itself and additional work is planned.

## 5 Future work

Regarding the knowledge of the PSFs, there is still work to be done. We are investigating the best way to parameterize the PSFs. From there, we must find solutions that are physically acceptable, define confidence intervals in our results, and see if the solutions we find are unique or not.

There is also an additional difficulty to consider. We have defined our function to minimize as  $FOM = FOM(\lambda_1, \lambda_2, \dots, \lambda_n)$ , implicitly assuming that each set of PSFs give rise to some specific cascades. Actually this is not so, since from the same level densities and PSFs different *realizations* of the same nucleus can be generated [16]. Thus, different cascades can be obtained for the same set of PSFs. For the moment, what we have done in our studies is to control the random number generators so that a certain set of  $\lambda$ -parameters always gives the same  $FOM$ , i.e., they always generate the same realization of the nucleus. However, this effect has to be considered in the future. We have verified that, for values close to the optimum, the variation in the value of the  $FOM$  with the realization is distributed similarly to a Gaussian with a standard deviation of 6-7%.

**Acknowledgements:** This work was supported in part by the Spanish national company for radioactive waste management ENRESA, through the CIEMAT-ENRESA agreements on “Transmutación de radionucleidos de vida larga como soporte a la gestión de residuos radioactivos de alta actividad”; by the Spanish Plan Nacional de I+D+i de Física de Partículas, through the projects FPA2017-82647-P and PGC2018-096717-B-C21; and by the European Commission with the FP7 project CHANDA (FP7-605203).

## References

- [1] C. Guerrero et al. (the n\_TOF Collaboration), The European Physical Journal A **49**, 27 (2013)
- [2] C. Guerrero et al. (the n\_TOF Collaboration), Nucl. Instrum. Methods A **608**, 424 (2009)
- [3] C. Weiß et al. (the n\_TOF Collaboration), Nucl. Instrum. Methods A **799**, 90 (2015)
- [4] V. Alcayne et al. (the n\_TOF Collaboration), EPJ Web Conf. **211**, 03008 (2019)
- [5] C. Guerrero et al. (the n\_TOF Collaboration), Journal of the Korean Physical Society **59**, 1510 (2011)
- [6] C. Guerrero et al. (the n\_TOF Collaboration), Phys. Rev. C **85**, 044616 (2012)
- [7] E. Mendoza et al. (the n\_TOF Collaboration), Phys. Rev. C **90**, 034608 (2014)
- [8] J. Balibrea-Correa et al. (the n\_TOF Collaboration), EPJ Web Conf. **146**, 11021 (2017)
- [9] E. Mendoza et al. (the n\_TOF Collaboration), Phys. Rev. C **97**, 054616 (2018)
- [10] J. Moreno-Soto et al. (the n\_TOF Collaboration), EPJ Web Conf. **211**, 02002 (2019)
- [11] J. Lerendegui-Marco et al. (the n\_TOF Collaboration), Phys. Rev. C **97**, 024605 (2018)
- [12] P.W. Lisowski et al., Nuclear Science and Engineering **106**, 208 (1990)
- [13] J.L. Ullmann et al., Phys. Rev. C **96**, 024627 (2017)
- [14] J.L. Ullmann et al., Phys. Rev. C **89**, 034603 (2014)
- [15] M. Jandel et al., Phys. Rev. C **78**, 034609 (2008)
- [16] F. Bečvář, Nucl. Instrum. Methods A **417**, 434 (1998)
- [17] D. Jordan, A. Algora, J. Tain, Nucl. Instrum. Methods A **828**, 52 (2016)
- [18] S. Agostinelli et al. (the GEANT4 Collaboration), Nucl. Instrum. Methods A **506**, 250 (2003)
- [19] C. Guerrero et al., Nucl. Instrum. Methods A **671**, 108 (2012)
- [20] M. Jandel et al., Nucl. Instrum. Methods B **261**, 1117 (2007)
- [21] <https://www.nndc.bnl.gov/ensdf/>
- [22] R. Capote et al., Nuclear Data Sheets **110**, 3107 (2009)
- [23] E. Mendoza et al., *NuDEX: a new nuclear  $\gamma$ -ray cascades generator*, in *2019 International Conference on Nuclear Data for Science and Technology* (submitted)
- [24] R. Storn, K. Price, Journal of Global Optimization **11**, 341 (1997)
- [25] S. Das, P.N. Suganthan, IEEE Transactions on Evolutionary Computation **15**, 4 (2011)
- [26] S. Das, S.S. Mullick, P. Suganthan, Swarm and Evolutionary Computation **27**, 1 (2016)